Iraqi J. Laser, issue 2, vol., 20, pp. 8-17 (2021)

IRAQI JOURNAL OF LASER

Parametric Optimization for Fatigue Life of 6061-T6 Aluminum Thin Sheets Processed with High-Speed Laser Shock Peening

Ali M. Khudhair[1,*], Furat I. Hussein[2]

*Corresponding author: ali.mohammed1201a@ilps.uobaghdad.edu.iq

1. *Institute of Laser for Postgraduate Studies, University of Baghdad, Iraq, Baghdad, Iraq.*
2. *Mechatronics Eng. Dep., Al-Khwarizmi College of Engineering, University of Baghdad, Baghdad, Iraq.*

(Received 11/10/2021; accepted 09/12/2021)

Abstract: Aluminum alloys grade 6061-T6 are characterized by their excellent properties and processing characteristics which make them ideal for varieties of industrial applications under cyclic loading, aluminum alloys show less fatigue life than steel alloys of similar strength. In the current study, a nanosecond fiber laser of maximum pulse energy up to 9.9 mJ was used to apply laser shock peening process (LSP) on aluminum thin sheets to introduce residual stresses in order to enhance fatigue life under cyclic loading Box-Behnken design (BBD) based on the design of experiments (DOE) was employed in this study for experimental design data analysis, model building and optimization The effect of working parameters spot size (ω), scanning speed (v) and pulse repetition rate (PRR) at three levels on the fatigue life expressed by the number of cycles (noc) were investigated The experimental results show an exclusive and significant percentage increase in the fatigue life of 505.25% and 477.81% when the ω= 0.04 mm and PRR= 22.5 kHz for two scanning speeds 200 mm/s and 500 mm/s respectively The optimized data extracted from the built model suggest a number of input parameters sets to enhance the performance of the process.

Keywords: fiber laser, aluminum alloy, LSP, high speed, DOE, fatigue.

1. Introduction

Aluminum alloys grade 6061-T6, are characterized by their good corrosion resistance, high strength-to-weight ratio and high toughness. Their excellent processing and welding characteristics make them ideal for varieties of industrial applications. Aluminum alloys find their ways widely in aircraft, automobiles, locomotives, couplings, marine, hydraulic pistons, appliance fittings, valves parts, bike frames and other industries [1, 2].

Under cyclic loading, aluminum alloys show less fatigue life than steel alloys of similar strength [3]. Laser shock penning (LSP) is introduced as one of a cold work surface treatment that enhances fatigue life [4]. Many research works revealed that mechanical properties such as tensile strength, hardness, wear resistance, and corrosion resistance are notoriously improved with LSP [5, 6]. Introducing residual stresses disrupt cracks growth rate and improve mechanical properties such as wear-resistance and fatigue life [7]. Short pulse lasers of high intensity (1 GW/cm^2) improve the surface strength and disrupt flaw propagation by imparting a layer of high compressive residual stresses [8, 9]. Even though nanosecond pulses are shorter than millisecond pulses, the interaction's nature remains thermal compared with shorter pulses such as femtosecond pulses [10, 11]. LSP is a process in which intense-short laser pulses pass through a transparent confining medium (such as water or glass) and focus on a metal surface covered with an absorbing layer. The latter may be an aluminum foil or black film that immediately vaporizes to form expanded plasma resulting in shockwaves against the processed metal followed by residual stresses and microstructure alterations [12]. When the pressure of the shockwave exceeds the material's dynamic yield strength, or HEL

(Hugoniot Elastic Limit), the material exhibits extremely high-stress deformation of about 10^6-10^7 GW/cm2 in a short time, causing local plastic deformation and compressive residual stresses [13].

Many research works investigate the role of LSP in enhancing the performance of cyclic operation for aluminum parts. Rubio-González et al. [14] evaluated the effect of different values of pulse densities on the residual stress field and fatigue crack initiation life. The study revealed higher pulse densities reduce fatigue crack growth and improve the fracture toughness characteristics for tested Al 6061-T6 alloy. Ahmed R. Alhamaoy et al. [15] had applied LSP to improve the cycle fatigue performance for Al 6061-T6 shafts coated with gel as an ablative layer without adding confining medium. Their results show a significant increase in the fatigue life when higher laser pulse energy is used. X. Q. Zhang et al. [16] applied two-sided LSP for Al 7050-T6 alloy to study residual stresses formation, surface feature and fatigue fracture morphology. The compressive residual stress cracks initiation and propagation rate. J. Shenget al. [17] utilized different laser pulse energies to study their effects on the crack propagation behavior for Al 6061-T6 alloy. They concluded that residual stresses caused by expanded plasma pressure could cancel tensile residual stress, reduce the notch driving force as well, and finally delay fatigue. Liu et. al., [18], has studied the effects of laser power density on the fatigue life of Al 7050 alloy subjected to LSP. Both the experimental and numerical results showed that a carefully chosen laser power density, when treating materials like aluminum alloys, can prevent internal cracking.

This paper aims to study the effects of manipulating LSP working parameters on the fatigue life of Al 6061-T6 alloy and utilize a statistical approach to develop a model capable of optimizing the working parameters of the process.

2. Experimental Work

An Al 6061-T6 thin plate was employed in this investigation. The chemical composition analysis (Table 1) was carried out at the Baghdad lab of the State Company for Inspection and Engineering Rehabilitation (SIER) in Baghdad. A tensile test was applied for a group of specimens to evaluate the mechanical properties of the alloy. The tensile specimens were cut and prepared according to the standard test method ASTM-E8 [19]. The tensile test was performed at speed of 2 mm/min using 100 kN Universal Testing Machine (Tinius Olsen (H100kU)\USA) under plane stress conditions.

Table (1) The Chemical Composition of Employed Al 6061-T6 Alloy

Element	The percentage ratio %
Si	00.677
Fe	00.548
Cu	00.236
Mn	00.131
Mg	00.844
Cr	00.179
Zn	00.0046
Ti	00.0787
P	00.0012
Pb	00.0094
Al	97.2

Table (2) lists some of the mechanical properties for the employed alloy according to the applied tensile test.

Table (2) Mechanical properties of Al 6061-T6

Property	Experimental
Yield Strength (MPa)	276
Ultimate Strength (MPa)	310
Elongation %	12%
Modulus of elasticity (GPa)	68.9

A thin plate of Al 6061-T6 of 1.6 mm thickness were cut in rectangular shapes of 10 mm × 100 mm dimensions according to the requirement of the fatigue testing device. Black paint was uniformly sprayed with a consistent thickness of 140 μm over the processed area on both sides of the specimen surface as a protective ablating layer as shown in figure (1a). A water layer of 2 mm to 3 mm height over the upper surface of the specimen was applied as a transparent confining layer and to support the built pressure by the plasma plume and reduce possible thermal effects. A nanosecond fiber laser model RFL-P\China (Figure (1b)) that was used in the current study has the following characteristics of 1064 nm wavelength, 81 ns pulse duration, max average power of 100 W and max pulse energy of 9.9 mJ.

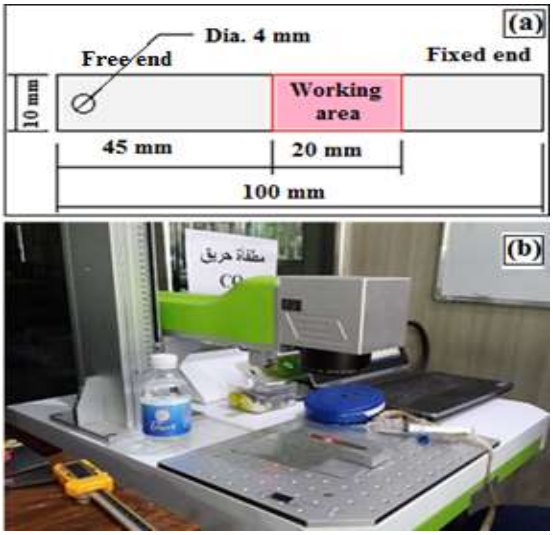

Figure (1): Experimental setup: **a)** fatigue test specimen final dimensions and state, **b)** specimen during processing

The laser beam was focused on the target with a focusing lens of 100 mm focal length and directed over the working area plane via Galvano mirrors with a high-speed reaching > 10000 mm/s maximum value. The irradiation pattern was in a one direction single pass with a variable overlap value along the laser beam direction and the constant overlapping ratio of 10% between two adjacent processed lines. The laser beam intensity in LSP should be high enough to cause plastic deformation in the metal surface. Here, the built pressure value (P) should be at least twice the yield strength value for the alloy. The sufficient value of laser beam intensity (I) can be calculated according to the following relation [20]:

$$P(GPa) = 0.01 \frac{\sqrt{a}}{2a+3} \sqrt{Z}\sqrt{I} \quad \ldots\ldots\ldots\ldots (1)$$

where *a* is the fraction of absorbed energy that contributes to the plasma's thermal energy and *Z* is the lower shock impedance between the metal and the confined fluid. [21, 22].

The fatigue test was carried out with the alternating bending device (type HSM20) by applying a predefined load for each specimen group at the free end of the specimen. Each experiment was conducted at room temperature using a constant load with zero mean stress and a frequency of 25 Hz. The produced specimens through the LSP process were classified according to the set of utilized working parameters. Each set was subjected to six tests of different fatigue stresses 263, 235, 222, 217, 210 and 205 MPa. Eighteen specimens were distributed for each fatigue stress sub-group. This makes the overall number for the seventeen groups of working parameters is 306 specimens.

3. Design of Experiments

Design of experiments (DOE) is a method for planning, carrying out, analyzing and interpreting experiments in a systematic way. DOE employs statistical tools to analysis the effect of input variables and their interactions on a response or group of responses. This approach decreases the number of experiments required to develop an experimental model that can be used to investigate the effect of process factors and their interactions on the response [22, 23]. Manipulating of input variables at the same time is possible with DOE to identify the important interactions that may be not observed when applying experiments with one factor at a time method [24]. Response surface methodology (RSM) is a mathematical and statistical technique based on DOE can efficiently model and analyze any process in which the response affected by input variables [25]. RSM can predict the response at various process variables as well as optimize it through find the values of variables that produces the best desired condition for the response [26] .

Design-expert v13 software package was used in current study to perform DOE, analyses data, build RSM model and optimize the process through Box-Behnken design (BBD). Optimization was benefit for predicting the optimum process variables that yields best fatigue life. In RSM, the general second-order polynomial model was used as a functional link between the independent variables and the response surface [27]:

$$Y = b_o + \sum_{i=1} b_{ii}\, x_i^2 + \sum_{i=1}^{n}. \sum_{j=i+1}^{n} b_{ij}\, x_i x_{j+e} \quad \ldots\ldots\ldots\ldots\ldots\ldots (2)$$

where *Y* is the response, the set *bo*, *bii* and *bij* are linear, quadratic and interaction regression coefficients, *xi* and *xj* are the independent variables and *e* is the experimental/residual error.

Design Expert ® V13 statistical software package from Stat-Ease Inc. was utilized to build the statistical model and analyze the obtained experimental data. BBD was used for three input independent variables namely the pulse repetition rate (PRR), laser spot size (ω) and scanning speed (v) on the dependent

response fatigue life. The range of input variable was designed and defined for the software to suggest the number and set of input variable for each experiment. Table (3) lists the lower and higher range for each input variable and their corresponding coded levels. The experiments were carried out to obtain the response values which inserted into the software later.

Table (3) Input parameters ranges and their coded levels

Variable	Actual values at coded levels		
	-1	0	+1
PRR (kHz)	20.00	22.5	25.00
ω (mm)	0.02	0.03	0.04
v (mm/s)	200.00	350	500.00

4. Results and Discussion

4.1 Experimental Results

The fatigue life values representing the responses are expressed by the number of cycles (noc) for each applied stress. The extracted experimental results for noc were inserted into DOE to finish data insertion. The experimental design considered three levels, three independent input parameters (PRR, ω, and v), and seventeen experiments. Table (4) presents the average fatigue life value of three specimens for each set of parameters group subjected to different loads as well as the raw metal noc values.

Table 4: BBD for extraction the response values for fatigue life.

Experiment No.	Parameters values (Coded values)			Responses: Average fatigue life (noc) × 10^4 (cycle)					
	PRR **(kHz)**	***ω*** **(mm)**	***v*** **(mm/s)**	**noc at 263 (Map)**	**noc at 235 (MPa)**	**noc at 222 (MPa)**	**noc at 217 (MPa)**	**noc at 210 (MPa)**	**noc at 205 (MPa)**
	Raw specimens (not processed)			4.273	9.229	10.749	12.286	15.077	18.508
1	22.5 (0)	0.03 (0)	350 (0)	5.636	9.633	18.468	28.078	38.794	46.812
2	22.5 (0)	0.03 (0)	350 (0)	6.052	13.098	20.233	30.226	43.900	57.098
3	25 (1)	0.04 (1)	350 (0)	4.701	10.717	20.381	30.267	41.874	57.619
4	25 (1)	0.03 (0)	500 (1)	8.568	15.770	21.818	30.688	43.413	51.920
5	25 (1)	0.03 (0)	200 (-1)	4.676	10.903	21.948	31.284	41.023	51.164
6	22.5 (0)	0.04 (1)	500 (1)	13.123	20.904	32.610	43.441	73.353	112.021
7	22.5 (0)	0.02 (-1)	500 (1)	3.760	9.598	19.013	24.047	30.297	38.351
8	20 (-1)	0.04 (1)	350 (0)	4.834	11.011	20.417	30.214	40.217	50.703
9	22.5 (0)	0.02 (-1)	200 (-1)	4.746	10.433	20.812	29.850	40.661	50.106
10	22.5 (0)	0.03 (0)	350 (0)	6.052	13.098	20.233	30.230	43.900	57.098
11	22.5 (0)	0.03 (0)	350 (0)	62.112	10.343	18.757	26.992	36.890	51.329
12	22.5(0)	0.03 (0)	350 (0)	5.120	11.250	13.601	22.551	31.489	50.226
13	20 (-1)	0.02 (-1)	350 (0)	4.378	9.569	20.191	30.144	31.727	54.378
14	20 (-1)	0.03 (0)	500(1)	4.046	10.253	19.050	23.986	34.063	44.319
15	20 (-1)	0.03 (0)	200 (-1)	4.691	11.914	22.453	29.870	40.263	49.000
16	22.5 (0)	0.04 (1)	200 (-1)	10.652	20.428	31.201	40.243	64.010	106.942
17	25 (1)	0.02 (-1)	350 (0)	4.378	9.569	20.191	30.144	31.723	54.378

Two of the applied experiments for different sets of input parameters show significant fatigue life: experiments 6 and 16. It could be deduced from both experiments the PRR of 22.5 and ω of 0.04 mm are the optimum operating conditions at the upper and lower scanning speed ω values of 200 mm/s and 500 mm/s. Compared with raw specimens, noc for these two sets of parameters recorded a percentage increase in fatigue life of 505.25% and 477.81% for experiments 6 and 16, respectively, as seen in figure (2).

The experimental data was represented on boxplot graphs to discover their variability or dispersion, outliers and symmetry. Boxplots graph in figure (3) show the impact of each input parameter at its three levels on data

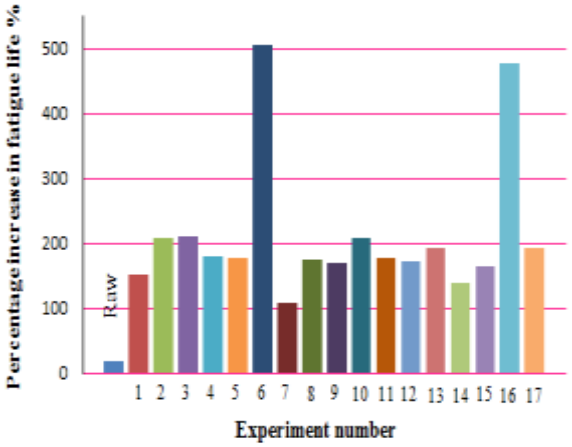

Figure (2): The percentage increase in fatigue life for the processed specimens at an applied stress of 205 MPa

characteristics and distribution. The high level of ω demonstrates more different amounts when compared with the other two parameters PRR and v, as seen in figure (3a). On the other hand, the other two levels of ω exhibit no effect of variability of the response and shorter whiskers. The more significant variability for noc data and wider whiskers can be observed at least for two levels of the v parameters as shown in figure (3b).

No outlier was observed where the whiskers length is shorter than the 1.5 times the interquartile range. The longer boxes of low and high levels for v indicates wider distribution, that is, more scattered data. Figure (3c) demonstrates less distribution and outlier data for the three levels of the parameters PRR. The median lines of the three boxplots overlap with their adjacent boxplots, and then there is likely to be no effective differences between the three levels.

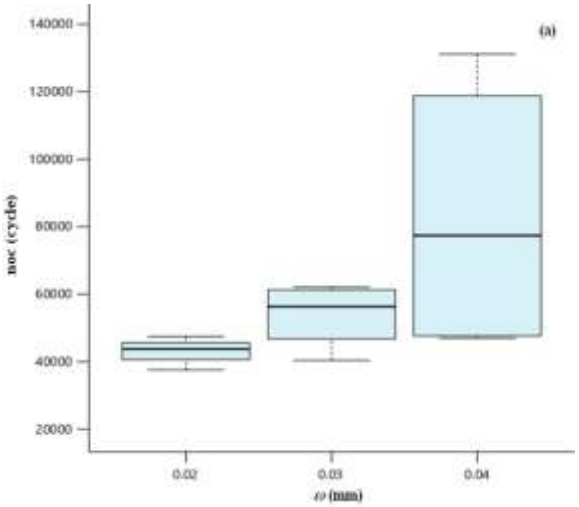

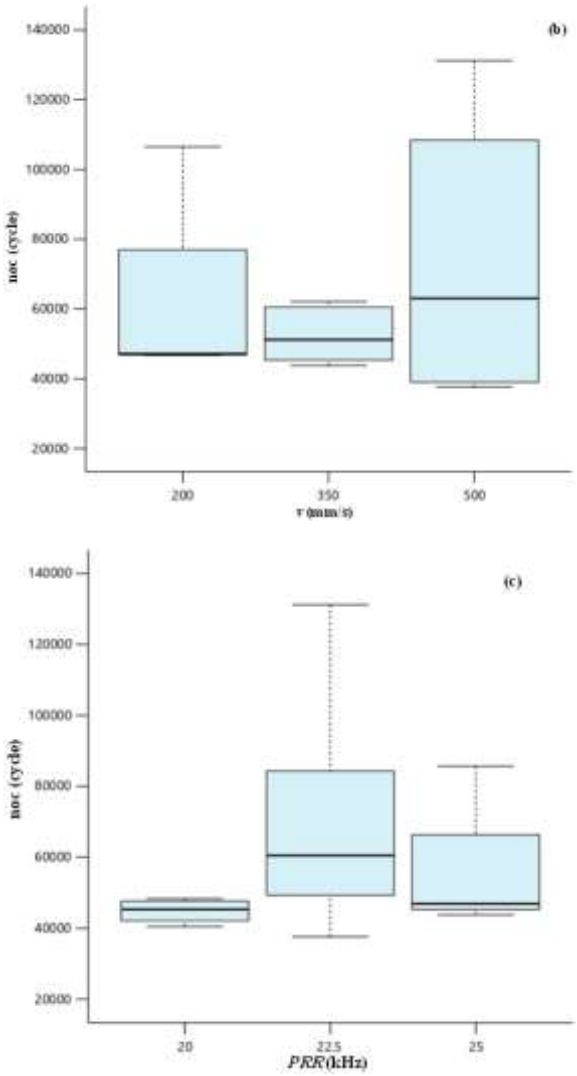

Figure (3): Boxplots representation for the distribution of data at three levels for each input parameter: a) spot size ω, b) scanning speed v and c) pulse repetition rate PRR.

For all three graphs, it can be seen that most of the boxplots for the three parameters are skewed (asymmetric) and don't follow a normal distribution.

4.2 Model Analysis

BBD based on RSM with three independent parameters as input variables and their interactions was utilized to develop the response surface models and their interactions. The response surface was tailored to fit the experimental results obtained from the executed experiments. The models predict found the responses noc at the various combination of working parameters PRR, ω and v. The adequate model without aliased terms after

eliminating some combinations of nominal and weird words.

Axiomatically, all of the responses for noc at different applied stresses show different values but approximately the same behavior when modeled. Thus, one of these models will be presented in the current section, reflecting the general conduct of fatigue lives at different applied stresses. The following analysis for the obtained model and optimization is related to the response at the applied pressure of 205 MPa. It is worth to mention the quadratic model was failed to represent the significance of the build model and its related input parameters. This may be related to the nature of obtained data in term of two significant results among almost the same level of data for the others. The cubic model handles the situation after elimination some diagnosed aliased combinations of input parameters. The mathematical model that benefits for predicting the response noc as a function of a set of the input parameters PRR, ω and *v* is as follow:

$$noc = -2.13 \times 10^{6} + 1.52 \times 10^{5}\, PRR + 7.72 \times 10^{6}\, \omega + 5.05 \times 10^{3}\, v - 114.11\, PRR.v - 89.3 \times 10^{3}\, \omega.v - 3.05 \times 10^{3}\, PRR^{2} + 1.7 \times 10^{8}\, \omega^{2} - 8.76\, v^{2} + 0.206\, PRR.v^{2} - 3 \times 10^{5}\, \omega^{2}.v + 161\, \omega.v^{2} \ldots\ldots\ldots (3)$$

One-way Analysis of variance test (ANOVA) was applied for the reduced cubic model given in table (5) to test the null hypothesis and analyze the statistically significant differences between the means of variables.

Table (5): ANOVA test for noc at applied stress of 205 MPa.

Source	Sum of Squares	df	Mean Square	*F*-value	*p*-value	
Model	1.013×10^{10}	11	9.207×10^{8}	58.36	0.0001	significant
PRR	4.469×10^{5}	1	4.469×10^{5}	0.0283	0.8729	
ω	1.514×10^{7}	1	1.514×10^{7}	0.9593	0.3723	
v	2.637×10^{8}	1	2.637×10^{8}	16.71	0.0095	
PRR . ω	5.146×10^{8}	1	5.146×10^{8}	32.62	0.0023	
ω . v	2.984×10^{8}	1	2.984×10^{8}	18.91	0.0074	
PRR^2	1.533×10^{9}	1	1.533×10^{9}	97.16	0.0002	
ω^2	1.870×10^{8}	1	1.870×10^{8}	11.85	0.0184	
v^2	1.063×10^{9}	1	1.063×10^{9}	67.36	0.0004	
PRR . v	2.691×10^{8}	1	2.691×10^{8}	17.06	0.0091	
$\omega.v^2$	3.896×10^{7}	1	3.896×10^{7}	2.47	0.1769	
$\omega^2 v$	2.624×10^{9}	1	2.624×10^{9}	166.3	<0.0001	
Residual	7.889×10^{7}	5	1.578×10^{7}			
Lack of fit	4.469×10^{5}	1	4.496×10^{5}	0.0228	0.8873	not significant
Pure error	7.844×10^{7}	4	1.861×10^{7}			
Cor Total	1.021×10^{10}	16				

The F-value of 58.36 for the developed model implies the model is significant. There is only a 0.01%chance that this large F-value occur due to noise. The observed significant p-value of 0.0001 makes both terms of the model are significant. Among the duration of three input parameters, the v is found effective for both F-value and p-value. Likewise, the combinations of input parameters were found significant except the term ω.v2 was insignificant where the p-values greater than 0.10. The Lack of Fit F-value of 0.0228 implies that the Lack of Fit is unimportant relative to the pure error. There is an 88.73% chance that a Lack of Fit F-value this large could occur due to noise. Non-significant lack of fit is a good value to the model fit.

The fit statistics reveal an R^2 value of 0.9923 close to unity and has good agreement with an adjusted R^2 value of 0.9753. The Adequate Precision (Adeq) value measures the signal to

noise ratio. The model shows an Adeq Precision value of 28.049, where a ratio greater than 4 is desirable. This can give an indication that the model could be used to navigate the design space. Figure (4) shows the distribution of the actual data points of the response depicted by the experiments on each run versus the predicted values evaluated by the model. It can be seen data points distributed along the 45o line indicating good agreement of experimental and expected results by the model.

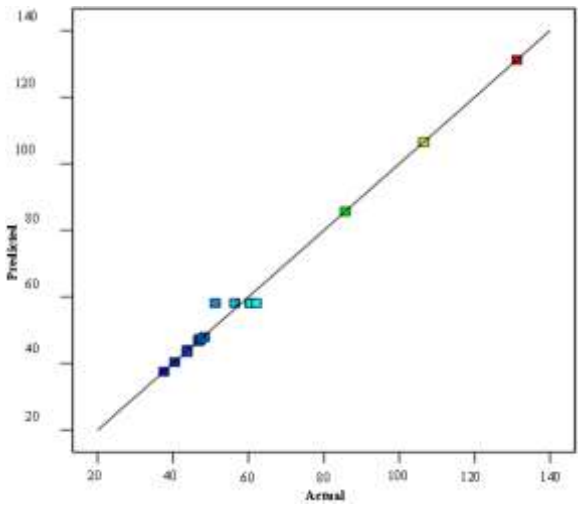

Figure (4): Plot of predicted vs. actual data of the modified model in noc.

According to the experimental results and statistical analysis, RSM plots the three-dimensional graphs for the response noc as a function of two or more input parameters. Figure 5 defines in 3D graph and contour plot the values of noc at a combination of two input parameters for a certain fixed value for the third one. The effect of PRR and ω for a fixed value of v 200 mm/s is illustrated in Figure 5a. The impact of PRR and ω on the fatigue life indicated that noc was maximum at ω=0.04 mm and PRR= 22.5 kHz. It is clear that noc has increased with increasing ω and PRR towards the maximum and moderate values respectively. For the same graph, if v switched to average values of 350 mm/s, the response surface decreases before increasing to the maximum at v=500 mm/s. High scanning speed results in a high cooling rate and low interaction time with the target, resulting in less roughness and high hardness.

However, when the speed declines, the interaction time increases, and the cooling rate decreases, resulting in increased surface roughness accompanied by lower hardness [28].

The effect of PRR and v on the response, at fixed value of ω=0.03 mm, is depicted in Figure 5b. Moving PRR from the moderate to high values gives higher values of noc at the terminals of v 200 mm/s and 500 mm/s. Changing the value of ω to the minimum lowers the response surface down and vice versa. The induced compressive residual stresses at the surface obviously increase for a certain depth with increasing ω [29].

The effect of ω and v on the noc when the PRR at 22 kHz is shown in figure (5c). The noc shows two significant peaks when ω= 0.04 mm and v is at the maximum or minimum values. Lowering the value of PRR lowers the response surface and keeps the same pattern. This may be related to plasma formation rule related to the laser intensities value. At low intensity of less than 1 GW/cm2 LSP is not verified. At moderate range of 1 GW/cm2 to 7 GW/cm2, the plasma pressure reaches its maximum limit. When the intensity increases above 7 GW/cm2, plasma saturation and light shielding occur [30].

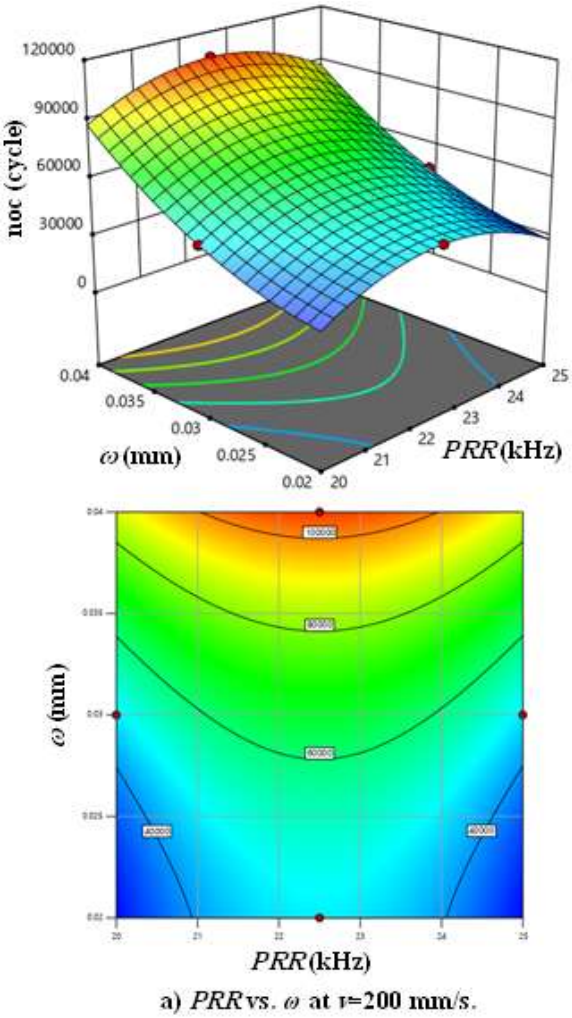

a) *PRR* vs. *ω* at v=200 mm/s.

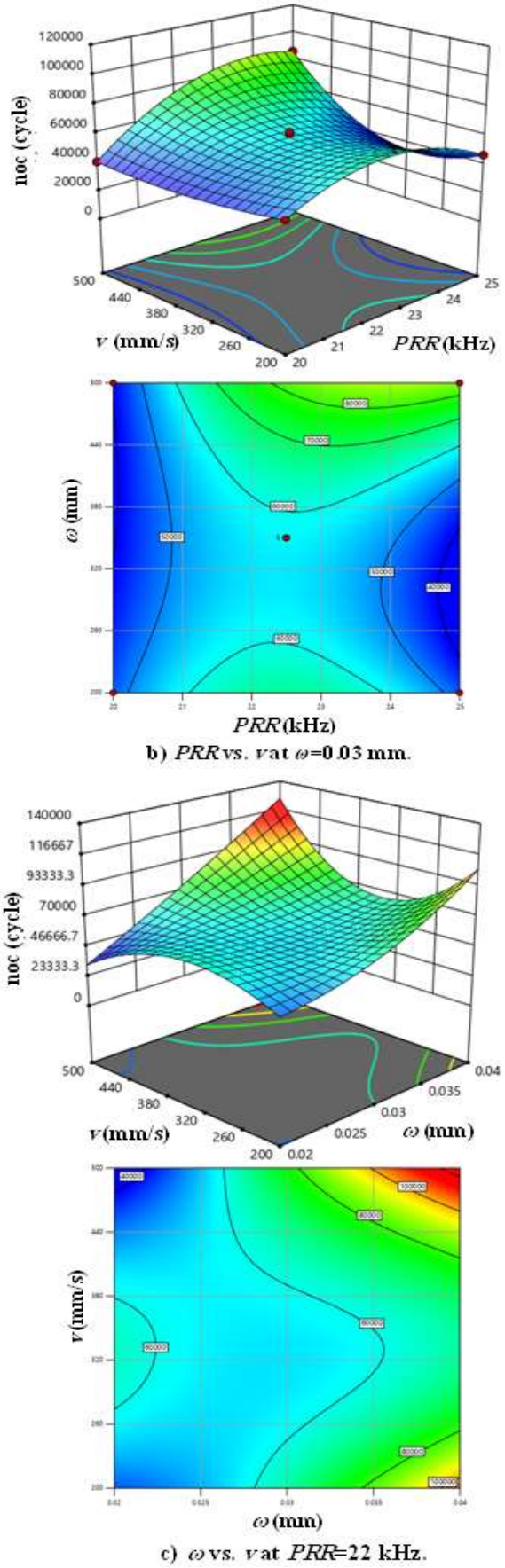

Figure (5): 3D response plots for noc.

4.3 Optimization

To enhance the fatigue life efficiency, the optimum suggested operating parameters were introduced by the model as shown in Figure 6. In the criteria of optimization, three optimized conditions were extracted out by setting three different criteria:

a) Maximum response could be attained for PRR range of 22 - 25 kHz and ω range of 0.035 – 0.04 mm when the experiment operates at v of 500 mm/s as shown in Figure 6a.

b) Figure 6b shows it is possible maximize the response through two conditions at constant value of ω equals to 0.04 mm and PRR range of 21 – 25 kHz. The highest one is when v equals 500 mm/s and the lowest one at v equals to 200 mm/s .

c) To maximize the response Figure 6c reveals two sets optimized conditions at PRR of 25 kHz. The largest one when the v equals 500 mm/s and ω=0.04 mm and the smaller one when the v equals 200 mm/s for same value of ω.

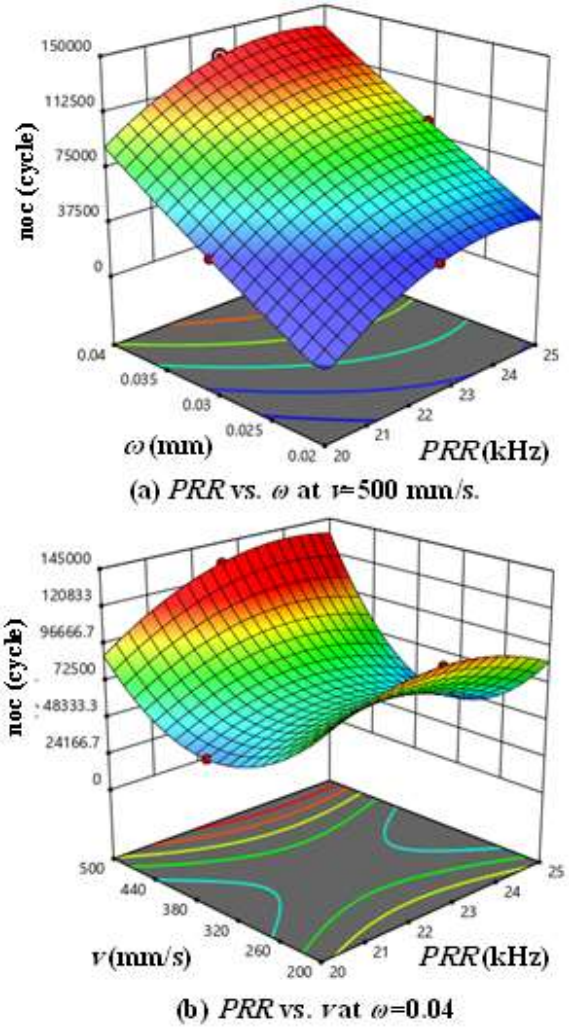

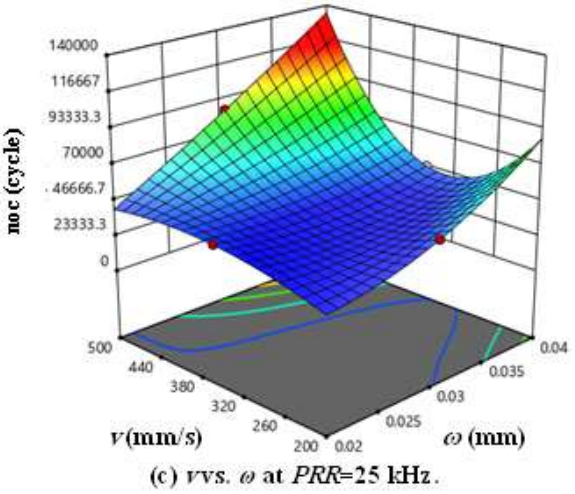

Figure (6): 3D response plots for desired response values.

5. Conclusions

LSP treatment for Aluminum 6061-T6 thin sheets, reveals a significant improvement in fatigue life under cyclic loading. The following concluded remarks are extracted from the current study:

1. Processing samples with LSP showed a variety range of improvement for the fatigue life with respect to the untreated samples. At two sets of input parameters, the results were highly considerable. When the PRR equals 22.5 kHz and ω was 0.04 mm the percentage increase in fatigue life was 505.25% and 477.81% at the minimum and maximum scanning speeds 200 mm/s and 500 mm/s respectively.
2. The experiments results show that both v followed by the ω are the most effective parameter reveal a wider variance in the fatigue life values represented by noc.
3. The quadratic model failed to explore the design space due to the few numbers of significant results (only two) which may be considered as noise. Therefore, experimental modeling switched toward the cubic model after terminating the aliased combination of parameters.
4. The presented model reveals a variety of conditions for improving the fatigue life results such as: when applying the v at 500 mm/sec for PRR range of 22 – 25 kHz and ω range of 0.035 – 0.04 mm. Another optimization set when the scanning speed v at its maximum or minimum limits at ω of 0.04 mm and PRR from 21 to 25 kHz.

6. Acknowledgment

The authors are grateful for the support provided by the Institute of Laser for Postgraduate Studies at University of Baghdad and Mechatronics Engineering Department, Al-Khwarizmi College of Engineering at University of Baghdad.

7. References

[1] R. I. Rodriguez, J. B. Jordon, P. G. Allison, T. Rushing, and L. Garcia, "Microstructure and mechanical properties of dissimilar friction stir welding of 6061-to-7050 aluminum alloys," Materials & Design, vol. 83. Elsevier BV, pp. 60–65, Oct. 2015. doi: 10.1016 /j.matdes.2015.05.074.

[2]S. Malopheyev, I. Vysotskiy, V. Kulitskiy, S. Mironov, and R. Kaibyshev, "Optimization of processing- microstructure- properties relationship in friction-stir welded 6061-T6 aluminum alloy," Materials Science and Engineering: A, vol. 662. Elsevier BV, pp. 136–143, Apr. 2016. doi: 10.1016 /j.msea. 2016.03.063.

[3] H. Hao, D. Ye, and C. Chen, "Strain ratio effects on low-cycle fatigue behavior and deformation microstructure of 2124-T851 aluminum alloy," Materials Science and Engineering: A, vol. 605. Elsevier BV, pp. 151–159, May 2014. doi: 10.1016/j.msea. 2014.03.040.

[4] J. P. Hirth, "Effects of hydrogen on the properties of iron and steel," Metallurgical Transactions A, vol. 11, no. 6. Springer Science and Business Media LLC, pp. 861–890, Jun. 1980. doi: 10.1007/bf02654700.

[5] C. Correa et al., "Random-type scanning patterns in laser shock peening without absorbing coating in 2024-T351 Al alloy: A solution to reduce residual stress anisotropy," Optics & Laser Technology, vol. 73. Elsevier BV, pp. 179–187, Oct. 2015. doi: 10.1016/j.optlastec.2015.04.027.

[6] U. Trdan, M. Skarba, and J. Grum, "Laser shock peening effect on the dislocation transitions and grain refinement of Al–Mg–Si alloy," Materials Characterization, vol. 97. Elsevier BV, pp. 57–68, Nov. 2014. doi: 10.1016/j.matchar.2014.08.020 .

[7] C. Montross, "Laser shock processing and its effects on microstructure and properties of metal alloys: a review," International Journal of

Fatigue, vol. 24, no. 10. Elsevier BV, pp. 1021–1036, Oct. 2002. doi: 10.1016/s0142-1123(02)00022-1 .
[8] R. Fabbro, P. Peyre, L. Berthe, and X. Scherpereel, “Physics and applications of laser-shock processing,” Journal of Laser Applications, vol. 10, no. 6. Laser Institute of America, pp. 265–279, Dec. 1998. doi: 10.2351/1.521861 .
[9] W. Guo et al., “Laser shock peening of laser additive manufactured Ti6Al4V titanium alloy,” Surface and Coatings Technology, vol. 349. Elsevier BV, pp. 503–510, Sep. 2018. doi: 10.1016/j.surfcoat.2018.06.020 .
[10]A. Issa, F. I. Hussein Al-Najjar, A. Al-Hamaoy, and B. G. Rasheed, “Physical principles of laser–material interaction regimes for laser machining processes,” Laser Micro- and Nano-Scale Processing. IOP Publishing, Aug. 2021. doi: 10.1088/978-0-7503-1683-5ch3.
[11]F. I. Hussein Al-Najjar, A. Al-Hamaoy, B. G. Rasheed, and A. Issa, “Effective working parameters of laser micro-/nano-machining,” Laser Micro- and Nano-Scale Processing. IOP Publishing, Aug. 2021. doi: 10.1088/978-0-7503-1683-5ch4.
[12] J. Zhao et al., “A rapid one-step nanosecond laser process for fabrication of super-hydrophilic aluminum surface,” Optics & Laser Technology, vol. 117. Elsevier BV, pp. 134–141, Sep. 2019. doi: 10.1016/j.optlastec.2019.04.015 .
[13] C.-Y. Shih et al., “Two mechanisms of nanoparticle generation in picosecond laser ablation in liquids: the origin of the bimodal size distribution,” Nanoscale, vol. 10, no. 15. Royal Society of Chemistry (RSC), pp. 6900–6910, 2018. doi: 10.1039/c7nr08614h.
[14] C. Rubio-González et al., “Effect of laser shock processing on fatigue crack growth and fracture toughness of 6061-T6 aluminum alloy,” Materials Science and Engineering: A, vol. 386, no. 1–2. Elsevier BV, pp. 291–295, Nov. 2004. doi: 10.1016/j.msea.2004.07.025.
[15]A. R. Alhamaoy, G. Sh. Sadiq, F. I. Hussein, and S. N. Ali, “The Cyclic Fatigue Behavior for 6061-T6 Al Alloy Shafts Processed by Laser Shock Peening,” Materials Science Forum, vol. 1002. Trans Tech Publications, Ltd., pp. 21–32, Jul. 2020. doi: 10.4028/www.scientific.net/msf.1002.21.
[16] X. Q. Zhang et al., “Investigation on effect of laser shock processing on fatigue crack initiation and its growth in aluminum alloy plate,” Materials & Design (1980-2015), vol. 65. Elsevier BV, pp. 425–431, Jan. 2015. doi: 10.1016/j.matdes.2014.09.001.
[17] S. Huang et al., “Effects of laser energy on fatigue crack growth properties of 6061-T6 aluminum alloy subjected to multiple laser peening,” Engineering Fracture Mechanics, vol. 99. Elsevier BV, pp. 87–100, Feb. 2013. doi: 10.1016/j.engfracmech.2013.01.011.
[18] Q. LIU, C. H. YANG, K. DING, S. A. BARTER, and L. YE, “The effect of laser power density on the fatigue life of laser-shock-peened 7050 aluminium alloy,” Fatigue & Fracture of Engineering Materials and Structures, vol. 30, no. 11. Wiley, pp. 1110–1124, Nov. 2007. doi: 10.1111/j.1460-2695.2007.01180.x .
[19] Standard Test Methods for Tension Testing of Metallic Materials
[20] T. Takata, M. Enoki, P. Chivavibul, A. Matsui, and Y. Kobayashi, “Effect of Confinement Layer on Laser Ablation and Cavitation Bubble during Laser Shock Peening,” MATERIALS TRANSACTIONS, vol. 57, no. 10. Japan Institute of Metals, pp. 1776–1783,2016.doi:10.2320/matertrans.m2016150.
[21] D. Devaux, R. Fabbro, L. Tollier, and E. Bartnicki, “Generation of shock waves by laser- induced plasma in confined geometry,” Journal of Applied Physics, vol. 74, no. 4. AIP Publishing, pp. 2268–2273, Aug. 15, 1993. doi: 10.1063/1.354710.
[22] P. K. Park, D. H. Cho, E. Y. Kim, and K. H. Chu, “Optimization of carotenoid production by Rhodotorula glutinis using statistical experimental design,” World Journal of Microbiology and Biotechnology, vol. 21, no. 4. Springer Science and Business Media LLC, pp. 429–434, Jun. 2005. doi: 10.1007/s11274-004-1891-3.
[23] L. M. Collins, J. J. Dziak, and R. Li, “Design of experiments with multiple independent variables: A resource management perspective on complete and reduced factorial designs.,” Psychological Methods, vol. 14, no. 3. American Psychological Association (APA), pp. 202–224, 2009. doi: 10.1037/a0015826.
[24] B. Durakovic, “Design of experiments application, concepts, examples: State of the art,” Periodicals of Engineering and Natural Sciences (PEN), vol. 5, no. 3. International University of Sarajevo, Dec. 28, 2017. doi: 10.21533/pen.v5i3.145.

[25]M. Kumari and S. K. Gupta, "Response surface methodological (RSM) approach for optimizing the removal of trihalomethanes (THMs) and its precursor's by surfactant modified magnetic nanoadsorbents (sMNP) - An endeavor to diminish probable cancer risk," Scientific Reports, vol. 9, no. 1. Springer Science and Business Media LLC, Dec. 2019. doi: 10.1038/s41598-019-54902-8.

[26] K. A. Mohamad Said and M. A. Mohamed Amin, "Overview on the Response Surface Methodology (RSM) in Extraction Processes," Journal of Applied Science & Process Engineering, vol. 2, no. 1. UNIMAS Publisher, May 12, 2016. doi: 10.33736/jaspe.161.2015.

[27] S. L. C. Ferreira et al., "Box-Behnken design: An alternative for the optimization of analytical methods," Analytica Chimica Acta, vol. 597, no. 2. Elsevier BV, pp. 179–186, Aug. 2007. doi: 10.1016/j.aca.2007.07.011 .

[28] N. R. Dhar and M. Kamruzzaman, "Cutting temperature, tool wear, surface roughness and dimensional deviation in turning AISI-4037 steel under cryogenic condition," International Journal of Machine Tools and Manufacture, vol. 47, no. 5. Elsevier BV, pp. 754–759, Apr. 2007. doi: 10.1016/j.ijmachtools.2006.09.018.

[29] Y. Liu, D. Xu, M. Agmell, A. Ahadi, J.-E. Stahl, and J. Zhou, "Investigation on residual stress evolution in nickel-based alloy affected by multiple cutting operations," Journal of Manufacturing Processes, vol. 68. Elsevier BV, pp. 818–833, Aug. 2021. doi: 10.1016/j.jmapro.2021.06.015.

[30] C. Montross, "Laser shock processing and its effects on microstructure and properties of metal alloys: a review," International Journal of Fatigue, vol. 24, no. 10. Elsevier BV, pp. 1021–1036, Oct. 2002. doi: 10.1016/s0142-1123(02)00022-1.

تحسين معلمات عمر الكلال لألواح الألومنيوم الرقيقة نوع T6-6061 المُعالجة بالسفع بالليزر فائق السرعة

علي محمد خضير[1] , فرات ابراهيم حسين[2]

[1] معهد الليزر للدراسات العليا/جامعة بغداد
[2] قسم هندسة الميكاترونكس/كلية الهندسة الخوارزمي/جامعة بغداد

الخلاصة: تتميز سبائك الألومنيوم نوع T6-6061 بخصائصها الممتازة ومزيا سهولة المعالجة التي تجعلها مثالية لأنواع مختلفة من التطبيقات الصناعية. تظهر سبائك الألومنيوم عند التحميل الدوري عمرا للكلال أقل من سبائك الصلب ذات الخواص الميكانيكية المماثلة. في الدراسة الحالية تم استخدام ليزر الألياف نوع النانوثانية بقدرة عالية تصل إلى 100 واط لتطبيق عملية سفع باالليزر على صفائح الألومنيوم الرقيقة لاضافة اجهادات داخلية من أجل تعزيز وزيادة عمر الفشل الكلالي تحت التحميل الدوري. في هذه الدراسة تم استخدام تصميم Box-Behnken (BBD) بناءً على اسلوب تصميم التجارب (DOE) لتحليل بيانات التصميم التجريبي وبناء النماذج المبنية على نتائج المختبر وتحسينها. تم التحقيق في تأثير معلمات التشغيل وهي حجم البقعة (ω) وسرعة المسح (v) ومعدل تكرار النبضات (PRR) بثلاثة مستويات مختلفة القيمة على عمر الكلال المعبر عنه بعدد الدورات اللازمة لحدوث الفشل (noc). أظهرت النتائج زيادة حصرية في عمر الكلال بنسب مئوية قدرها 505.25٪ و 477.81٪ عند ω = 0.04mm و PRR = 22.5kHz لسرعتي المسح 200 mm/s و 500 mm/s على التوالي. تم الحصول من النموذج التطبيقي المبنى عدة مقترحات لمعلمات الادخال التي من الممكن ان تحسن المخرجات و أداء العملية متمثلة بعمر كلال أعلى.